ORIGINAL ARTICLE

Time-dependent recovery of brain hypometabolism in neuro-COVID-19 patients

Anna Lisa Martini[1] · Giulia Carli[2] · Lorenzo Kiferle[3] · Patrizia Piersanti[3] · Pasquale Palumbo[3] · Silvia Morbelli[4,5] · Maria Lucia Calcagni[6] · Daniela Perani[7,8,9] · Stelvio Sestini[1]

Abstract

Purpose We evaluated brain metabolic dysfunctions and associations with neurological and biological parameters in acute, subacute and chronic COVID-19 phases to provide deeper insights into the pathophysiology of the disease.

Methods Twenty-six patients with neurological symptoms (neuro-COVID-19) and [^{18}F]FDG-PET were included. Seven patients were acute (< 1 month (m) after onset), 12 subacute ($4 \geq 1$-m, $4 \geq 2$-m and $4 \geq 3$-m) and 7 with neuro-post-COVID-19 ($3 \geq 5$-m and $4 \geq 7$–9-m). One patient was evaluated longitudinally (acute and 5-m). Brain hypo- and hypermetabolism were analysed at single-subject and group levels. Correlations between severity/extent of brain hypo- and hypermetabolism and biological (oxygen saturation and C-reactive protein) and clinical variables (global cognition and Body Mass Index) were assessed.

Results The "fronto-insular cortex" emerged as the hypometabolic hallmark of neuro-COVID-19. Acute patients showed the most severe hypometabolism affecting several cortical regions. Three-m and 5-m patients showed a progressive reduction of hypometabolism, with limited frontal clusters. After 7–9 months, no brain hypometabolism was detected. The patient evaluated longitudinally showed a diffuse brain hypometabolism in the acute phase, almost recovered after 5 months. Brain hypometabolism correlated with cognitive dysfunction, low blood saturation and high inflammatory status. Hypermetabolism in the brainstem, cerebellum, hippocampus and amygdala persisted over time and correlated with inflammation status.

Conclusion Synergistic effects of systemic virus-mediated inflammation and transient hypoxia yield a dysfunction of the fronto-insular cortex, a signature of CNS involvement in neuro-COVID-19. This brain dysfunction is likely to be transient and almost reversible. The long-lasting brain hypermetabolism seems to reflect persistent inflammation processes.

This article is part of the Topical Collection on Neurology.

Anna Lisa Martini and Giulia Carli contributed equally.

✉ Stelvio Sestini
 stelvio.sestini@uslcentro.toscana.it

1 Nuclear Medicine Unit, Department of Diagnostic Imaging, N.O.P. - S. Stefano, U.S.L. Toscana Centro, Prato, Italy

2 Department of Nuclear Medicine and Molecular Imaging, University of Groningen, University Medical Center Groningen, Groningen, the Netherlands

3 Neurology Unit, N.O.P. - S. Stefano, U.S.L. Toscana Centro, Prato, Italy

4 Nuclear Medicine Unit, IRCCS Ospedale Policlinico San Martino, Genoa, Italy

5 Department of Health Sciences, University of Genoa, Genoa, Italy

6 Nucler Medicine Unit Policlinico Universitario A. Gemelli, IRCCS, Rome, Italy

7 School of Psychology, Vita-Salute San Raffaele University, Milan, Italy

8 In Vivo Human Molecular and Structural Neuroimaging Unit, Division of Neuroscience, IRCCS San Raffaele Scientific Institute, Milan, Italy

9 Nuclear Medicine Unit, San Raffaele Hospital, Milan, Italy

🕿 Springer

Introduction

A wide range of neurological manifestations is reported in association with coronavirus disease (COVID-19) (e.g. anosmia, hypogeusia, headache, cognitive deficits and altered consciousness) [1, 2]. COVID-19 patients can be classified based on the time onset of disease as patients in the acute ($<$ 1 month after the infection) and subacute phases (between 1 and 3 months after the infection) [3]. When symptoms persist for longer and are not explained by an alternative diagnosis, they are referred to the post-COVID-19 syndrome [4], or, as more recently suggested, to Neuro-PACS (neurological manifestations of post-acute sequelae of severe acute respiratory syndrome coronavirus 2 (SARS-CoV-2) infection) [5]. The mechanisms underlying the brain involvement in COVID-19 are still unclear. It is highly debated whether the virus can directly infect central (CNS) and peripheral nervous systems (PNS) [2], or if the "neurotoxicity" may result from indirect immune-mediated mechanisms (e.g. hyper-inflammation, autoimmune processes [6], hypoxemia, hypoperfusion, dehydration, glucose dysregulation and sedation effects of the acute phase [7–9]).

In this context, the [18F]-fluorodeoxyglucose position emission tomography (FDG-PET) has provided in vivo evidence of the brain pathophysiological involvement in COVID-19 patients [3, 10]. Previous [18F]FDG-PET studies investigated COVID-19 patients according to the timing of neurological symptoms [11–15], often focusing on one specific neurological manifestation (e.g. hyposmia) [11, 16–18]. Only one [18F]FDG-PET study has longitudinally evaluated the brain vulnerability in COVID-19-related encephalopathy, showing a frontal hypometabolism in the acute phase improving 6 months later [11]. Despite these promising results, further data are needed to explain CNS involvement in the pathophysiological mechanisms.

The present study aimed to characterise the time-dependent brain functional changes within the first year after COVID-19 infection in a series of patients with newly originated neurological symptoms (neuro-COVID-19). For the first time, we considered the currently available classifications of neuro-COVID, which refers to the onset timing of neurological symptoms [3]. For this purpose, we included patients with brain [18F]FDG-PET scans acquired in the acute (within 4 weeks) and sub-acute (1, 2, 3 months) phases, as well as during the post-COVID-19 syndrome (5, 7 and 9 months). One patient was followed longitudinally, with two [18F]FDG-PET brain scans (during the acute phase and 5 months later). All cases had measurements of clinical (global cognition and Body Mass Index) and biological parameters (oxygen saturation and C-reactive protein) that we correlated with brain metabolism changes

over time. All the above can provide deeper insights into the pathophysiology of brain involvement in COVID-19.

Materials and methods

Participants

We included patients affected by SARS-CoV-2 infection with new-onset neurological symptoms (e.g. disorientation, confusion, headache, sleepless, depressed mood, anxiety, delirium, chronic fatigue syndrome, hyposmia, ageusia) (Table 1 and S1). Some patients also presented cognitive disturbances (e.g. short-term memory, executive and visuo-spatial impairments) (Table 2). These patients were prospectively recruited in the Neurology Unit of Ospedale Santo Stefano Prato, Italy, from October 2020 to November 2021. As part of their clinical investigation, all patients underwent an [18F]FDG-PET brain scan. The COVID-19 infection was confirmed for all patients by a positive RT-PCR assay from a nasopharyngeal swab sample. Twenty-six neuro-COVID-19 patients (age 73.71 ± 11.28 years; 12/14 male/female; all right-handed) included in the present study fulfilled specific inclusion and exclusion criteria (S1). We classified patients according to the most widely accepted classification of COVID-19-related symptoms, which refers to their timing concerning infection [3]. Therefore, seven patients were examined in the acute phase (e.g. patients showing severe neurological impairment in addition to respiratory and systemic illness with multiple organ involvement during hospitalisation within 1 month from infection and symptoms onset), four during each subacute phase (1 month, 2 months, and 3 months) (e.g. patients with persistent neurocognitive symptoms beyond 1–3 months SARS-CoV-2 infection) and three and four in the neuro-post-COVID-19 at 5 and 7–9 months, respectively (e.g. patients with persistent neurocognitive symptoms beyond 3 months from infection and onset of symptoms). One patient was evaluated longitudinally during the acute phase and at a 5-month follow-up.

We included 125 healthy control (HC) from the AIMN (Associazione Italiana di Medicina Nucleare ed Imaging Molecolare) database on the AIMN website (https://aimn.it/brain-fdg/) (age, mean $\pm$ standard deviation (SD): 65.78 ± 11.33; Sex: 58 male/67 female, education, mean $\pm$ SD: 10.5 ± 4.29). This HC dataset has been previously validated for extracting SPM-based brain metabolism maps in patients [19]. These subjects were characterised by the absence of global cognitive impairment (Minimental State examination (MMSE), mean $\pm$ SD: 28.75 ± 1.69), and cognitive stability after an average 4-year clinical follow-up.

The present study was approved by the local ethics committee of the Nuclear Medicine Unit, Ospedale Santo Stefano Prato, Italy (N. 763, 29/03/2022), and complies

Table 1 Demographic clinic and cognitive features of SARS-CoV-2 patients

	Acute N=7	1-m N=4	2-m N=4	3-m N=4	5-m N=3	7/9-m N=4	p-value
Age (mean±SD)	73.71±11.28	71.5±8.70	68.5±10.79	64.25±14.41	80.67±80.02	67.25±10.31	p=0.449a
Gender (M/F)	2/5	2/2	4/0	1/3	2/1	0/4	p=0.069c
Hyposmia (Y/N)	6/1	4/0	3/1	4/0	2/0*	4/4	p=0.342c
Ageusia (Y/N)	5/2	2/2	1/2*	3/1	1/1*	3/1	p=0.614c
Blood saturation (mean±SD)	95.00±1.41	96.75±1.5	95.25±1.26	98.00±0.87□■	98.33±0.58 □■	98.5±0.58□■	p=0.003b
CRP (mean±SD)	21.41±9.54	2.4±0.41□	4.54±2.22	1.88±0.15□■	2.63±0.20	1.45±0.37□■ φ	p=0.000b
MMSE corrected scores (mean±SD)	n.a	23.25±1.26	23.75±0.96	28.00±1.41 φ■	29.33±1.41φ■	28.75±1.26 φ ■	p=0.006b
BMI (mean±SD)	27.63±3.76	25.83±1.84	29.25±2.46	25.90±0.96	26.58±0.52	24.35±1.40	p=0.129a
Hypometabolism extension (n° voxel)	52,190.14±32,193.40	47,318.50±15,218.81	40,131.50±25,459.47	9646.00±2804.42□	28,242.67±7496.95	4183.75±7204.36	p=0.003b
Hypometabolism hallmark severity (mean)	1.19±0.39	1.12±0.61	1.06±0.61	0.33±0.07□ φ■	0.71±0.24	−0.01±0.14□ φ ■€	p=0.001a
Hypermetabolism extension (n° voxel)	39,069.29±20,543.36	50,025.25±14,828.54	28,966.5±17,702.27	12,639.5±10,791.79	48,275.67±46,243.12	18,971.25±10,736.48	p=0.117a
Hypermetabolism hallmark severity (mean)	0.71±0.37	0.96±0.19	0.71±0.57	0.26±0.31	0.82±0.55	0.37±0.33	p=0.161a

1-m, 1 month after infection; *2-m*, 2 months after infection; *3-m*, 3 months after infection; *5-m*, 5 months after infection; *7-9-m*, 7–9 months after infection; *SD*, standard deviation; *M*, male; *F*, female; *CRP*, C-reactive protein; *BMI*, body mass index; *n°*, number; *n.a.* =not available. *For one patient, the information was not available. a: Oneway ANOVA with LSD correction for multiple comparisons. b: Kruskal–Wallis test with Bonferroni correction for multiple comparisons. c: Chi-squared test. Post-hoc comparison *p* < 0.05: □ Significantly differed from acute patients; φ significantly differed from 1-m patients; ■ significantly differed from 2-m patients; € significantly differed from 5-m patients

with Helsinki Declaration. Written informed consent was obtained from all patients.

Clinical and cognitive examination

Expert neurologists conducted neurological assessments as part of the clinical routine. The clinical examination included medical history and evaluation of some biological parameters, including values of C-reactive protein (CRP) as a measure of the inflammatory marker, blood saturation (SatO2%) and Body Mass Index (BMI) which were collected for each patient. The global cognitive functioning was tested throughout the Mini-Mental State Examination (MMSE) in 19 out of 26 patients. More extended neuropsychological evaluation was obtained in a subgroup of patients (11/26). Due to critical health conditions, the MMSE and neuropsychological battery were not tested in acute patients (S2).

[18F]FDG-PET image acquisition and pre-processing

All COVID-19 patients underwent an [18F]FDG-PET scan at rest as part of the clinical routine in the Nuclear Medicine Unit of S. Stefano Hospital-Azienda Toscana Centro, according to a specific protocol and the Italian/European guidelines [20]. The [18F]FDG-PET acquisition procedures conformed to the European Association of Nuclear Medicine (EANM) guidelines [21]. After an intravenous injection of 185–250 MBq of [18F]FDG, the patients were positioned comfortably in a quiet and dimly lit room several minutes before [18F]FDG administration and during the uptake phase of [18F]FDG for 45 min and, whenever possible, were instructed not to speak or be otherwise active. Thereafter, patients' images of the brain were acquired from a list-mode 15-min emission scan (one-bed position covering a 21.6-cm field of view along the z-axis) using a combined PET/CT system with a full-ring dedicated PET scanner (4–5 mm full-width half-maximum) and a 6-slice CT scanner (Biograph 6 True Point, Siemens, Erlangen, Germany). PET raw data were reconstructed into slices of 1.01 mm size spacing using "TrueX" iterative reconstruction 336×336 pixels, 6 iterations and 21 subsets, taking into account system point-spread function, modelled scatter and attenuation correction from non-contrast-enhanced CT with 130 kV, 11 mAs, 1.5 mm slice spacing and pitch 0.75.

As for the patients and HC, [18F]FDG-PET brain studies were performed according to EANM guidelines [21]. Before radiopharmaceutical injection, subjects were fasted for at least 6 h to ensure that the measured blood glucose level was < 120 mg/dL. Subjects underwent a 3D PET scan (time interval between injection and scan start ranged from 30 to 45 min; scan duration ranged from 10 to 15 min depending on the PET scanner characteristics) after the injection of [18F]FDG (185–250 MBq: usually, 5–8 mCi via a venous cannula). [18F]FDG PET images belonging

Table 2 Neuropsychological assessment in a subgroup of SARS-CoV-2 patients

	Cutoff	1-m N = 2 out of 4	2-m N = 3 out of 4	3-m N = 2 out of 4	5-m N = 2 out of 3	7/9-m N = 2 out of 4	p-value
Attentional matrices	< 31.00	39.00 ± 2.83	41.00 ± 17.35	58.50 ± 2.12	38.50 ± 4.95	43.00 ± 1.41	p = 0.216
Raven coloured progressive matrices	< 18.00	22.00 ± 1.41	24.49 ± 3.79	32.25 ± 1.06	25.70 ± 0.99	25.75 ± 2.47	p = 0.189
TMT A	> 127	48.50 ± 2.12	39.00 ± 7.81	26.50 ± 3.54	42.50 ± 0.71	36.50 ± 13.44	p = 0.153
TMT B	> 294	139.00 ± 2.83	120.00 ± 10.00	81.00 ± 1.41	135.00 ± 7.07	120.00 ± 1.41	p = 0.079
TMT B-A	> 163	90.50 ± 0.71	81.00 ± 4.58	54.50 ± 2.12	92.50 ± 7.78	83.50 ± 16.26	p = 0.148
Symbol digit	> 34.2	56.00 ± 1.41	60.00 ± 8.71	47.55 ± 0.78	59.20 ± 0.00*	50.20 ± 14.57	p = 0.525
Verbal fluency with phonemic cue	< 17.00	26.00 ± 1.41	<u>15.27 ± 0.46</u>	31.50 ± 0.71	24.50 ± 9.19	30.90 ± 0.28	p = 0.085
Verbal fluency with semantic cue	< 25.00	29.20 ± 2.12	30.33 ± 12.66	36.00 ± 1.41	32.50 ± 4.95	27.00 ± 16.97	p = 0.843
Digit span forward	< 4.26	<u>2.95 ± 0.07</u>	<u>2.98 ± 0.07</u>	5.50 ± 0.70	4.65 ± 0.49	4.68 ± 2.23	p = 0.096
RAVLT immediate recall	< 28.53	<u>19.25 ± 0.35</u>	<u>24.33 ± 4.76</u>	41.35 ± 1.91	29.27 ± 5.56	32.60 ± 17.68	p = 0.228
RAVLT delayed recall	< 4.69	6.1 ± 0.14	7.63 ± 0.81	7.6 ± 0.85	8.04 ± 0.08	9.35 ± 4.17	p = 0.334
Short story test immediate recall	< 3.10	4.15 ± 0.21	5.07 ± 0.12	3.80 ± 0.42	5.20 ± 0.28	5.25 ± 1.48	p = 0.167
Short story test delayed recall	< 2.39	3.15 ± 0.21	3.60 ± 0.69	5.55 ± 1.48	6.05 ± 1.34	4.75 ± 2.19	p = 0.190
ROCF immediate recall	< 6.44	12.75 ± 2.61	12.23 ± 2.54	18.00 ± 1.41	11.40 ± 0.00	16.55 ± 2.05	p = 0.126
ROCF delayed recall	< 9.47	16.10 ± 1.56	17.13 ± 1.86	13.35 ± 0.78	14.65 ± 0.92	18.30 ± 2.12	p = 0.153
ROCF copy	< 28.88	<u>27.95 ± 1.63</u>	28.00 ± 2.00	33.15 ± 1.63	29.60 ± 3.39	<u>27.55 ± 2.62</u>	p = 0.307
CD	< 7.18	11.50 ± 2.12	8.90 ± 0.85	8.65 ± 0.92	11.00 ± 0.00*	10.95 ± 1.48	p = 0.136
CDL	< 61.85	68.50 ± 2.12	66.43 ± 4.87	71.15 ± 1.20	70.10 ± 1.56	69.81 ± 3.31	p = 0.705

RAVLT, Rey Auditory Verbal Learning Test; *ROCF*, Rey–Osterrieth complex figure; *1-m*, 1 month after the infection; *2-m*, 2 months after the infection; *3-m*, 3 months after the infection; *5-m*, 5 months after the infection; *7–9-m*, 7–9 months after the infection; *SD*, standard deviation; *TMT*, trail making test; *CD*, freehand copying of drawings; *CDL*, copying drawing with landmarks. Data are given as mean ± SD. We used cutoff scores derived from normative data of the Italian population. The means under pathological cutoff are underlined in the table

to AIMN database were obtained using either a PET/CT system GE Discovery STE, GE Discovery 710 or Siemens Biograph 16 scanner [19].

Each reconstructed image was visually inspected to check for significant artefacts. Image pre-processing was performed using SPM12 software (http://www.fil.ion.ucl.ac.uk/spm/software/spm12/), running in Matlab (MathWorks Inc., Sherborn, MA, USA). First, each [18F]FDG-PET image was spatially normalised to a specific [18F]FDG-PET template in the MNI space [22]. Images were then spatially smoothed with an isotropic 3D Gaussian kernel of FWHM: 10–10-10 mm instead of 8–8-8 mm, to account for differences in reconstruction algorithms, according to literature guidelines [23]. Proportional global mean scaling was applied to each image [24]. In the SPM community, the proportional mean scaling is generally accepted as the most appropriate scaling method for [18F]FDG-PET images [25, 26]. This method implicitly assumes that the putative local changes detected do not significantly affect the global mean uptake of glucose. However, to definitively exclude the presence of artefacts due to the scaling approach, we compared the global mean metabolism uptake of patients and HC (S3), extracting the raw metabolic values from an [18F]FDG-PET specific mask. The absence of significant differences prevents underestimating hypometabolism and overestimating hypermetabolism with SPM-based statistical analyses.

Single-subject and group-level [18F]FDG-PET statistical parametric mapping analyses

This optimised SPM procedure possessed has been proven to have high sensitivity and reliability in detecting brain metabolic alterations at the single-subject level using statistical comparison with a large and well-selected database of HC (n = 125) (statistical threshold set at p = 0.05 uncorrected at voxels level, with cluster extent (Kep) ≥ 100 voxels) [19, 22, 24, 27]. We demonstrated that the SPM-based analysis procedure is affected neither by different scan acquisitions [27] nor by using different HC databases [19].

We also investigated the metabolic alterations at the group level using a statistical comparison between each group (within acute, 1-m, 2-m, 3-m, 5-m and 7–9-m phases) and HC. The statistical threshold was set at T-score 1.66 (p = 0.05 uncorrected at voxels level, FWE-corrected for multiple comparisons at clusters level, K > 100 voxels). Age was entered as a nuisance variable in both two-sample t-test models implemented in SPM12. Voxel-wise comparisons were made using a within-brain comparison-specific explicit [18F]FDG mask to remove emission counts outside the brain and cerebrospinal fluid voxels to restrict subsequent analyses to within-brain voxels. The SPM single-subject procedure provides SPM t-maps and contrast images showing regions of hypo- and hypermetabolism with a level of significance

corrected for age. Brain hypo- and hypermetabolism extension in each patient was quantified as the number of voxels in each binarized SPM T-map.

Brain hypo- and hypermetabolic hallmarks at group level

Brain hypo- and hypermetabolism commonalities were obtained in the whole group ($N = 26$) using a one-sample *t*-test entering the contrast images resulting from a first-order [^{18}F]FDG-PET SPM-based procedure (hypo- and hypermetabolic hallmarks) implemented in SPM12. The statistical threshold was set at T-score 1.66 ($p = 0.05$ uncorrected at voxels level, FWE-corrected for multiple comparisons at clusters level, K > 100 voxels). We then quantified the severity of hypo- and hypermetabolism in these specific regions of interest (ROIs) for each patient by extracting the mean value from contrast images resulting from a first-order [^{18}F]FDG-PET SPM-based procedure (quantification of hypo- and hypermetabolism severity). We also performed a voxel-wise group analysis to obtain the common pattern of brain hypo- and hypermetabolism in each group divided according to the disease phase as previously mentioned (i.e. acute, 1-m, 2-m , 3-m , 5-m and 7–9-m). Specifically, we obtained the common hypo- and hypermetabolism patterns by comparing each group with HC ($N = 125$) through a *t*-test statistical comparison on SPM12, controlling for age.

Statistical analyses

We performed the analysis of variance (ANOVA) for normally distributed variables and the Kruskal–Wallis test for non-parametric variables to study clinical (BMI), cognitive (MMSE), bio-humoral (SaT02%, CRP) and metabolic differences among groups (acute, 1-m, 2-m , 3-m , 5-m and 7–9-m). We also evaluated the relationship between such variables of interest (i.e. blood saturation, CRP, MMSE and BMI) and extent/severity of hypometabolic findings using Spearman correlation analyses. Last, we evaluated whether global cognitive efficiency (MMSE), age, SatTO02%, CRP and BMI could predict the extent and severity of hypo- and hypermetabolic findings using linear regression models. The significance threshold was set at $p \leq 0.05$. We performed all statistical analyses using SPSS version 26.0 (IBM Corp., Armonk, NY).

Results

Clinical and cognitive features

The groups cross-sectionally showed significant differences in SatO2%, CRP values and MMSE corrected scores; the acute phase showed the most severe values that gradually improved across groups (Table 1). Acute and sub-acute patients (2-m) showed significantly lower saturation than 3-m ($p_{acute} = 0.012$ and $p_{2-m} = 0.022$), 5-m ($p_{acute} = 0.009$ and $p_{2-m} = 0.015$) and 7–9-m patients ($p_{acute} = 0.002$ and $p_{2-m} = 0.005$). The acute patients showed a significantly higher inflammatory levels compared to 1-m ($p = 0.027$), 3-m ($p = 0.000$) and 7–9-m patients ($p = 0.000$) and the 2-m patients compared to 7–9-m ones ($p = 0.013$). Also, MMSE's performance improved over time. Both 1-m and 2-m patients showed significant lower MMSE scores than 3-m ($p_{1-m} = 0.032$), 5-m ($p_{1-m} = 0.004$ and $p_{2-m} = 0.011$) and 7–9-m patients ($p_{1-m} = 0.007$ and $p_{2-m} = 0.018$). Altered performances in neuropsychological tests, namely in the executive domain (digit forward and RAVLT immediate recall corrected scores), emerged only in the sub-acute phases (1-m and 2-m) (Table 2). Three months and onward, patients showed cognitive performances within the normal range. See Table S1 in supplementary materials for the prevalence of neurological symptoms across groups.

Concerning the longitudinal case report, the patient followed longitudinally showed a significant improvement in saturation and inflammatory levels from the acute phase (SatO2% = 92 and CRP = 30.5) to the 5 months follow-up (SatO2% = 98 and CRP = 2.83). The patient also showed a normal global cognitive cognition at the follow-up (MMSE corrected score = 28); in the acute phase, it was not performed due to a critical health condition. The patient presented with persistent hyposmia and ageusia (Fig. 1).

Patterns of [^{18}F]FDG-PET hypo- and hypermetabolism

All groups showed comparable global metabolism uptake values. Also, the comparison between the whole patient cohort ($N = 26$) and HC showed no significant differences ($p = 0.253$) (Table S2).

Hypometabolism hallmark at group level

The hypometabolism commonality analysis showed the fronto-insular cortex as the hypometabolic hallmark for the "whole group", with more limited involvement of the parietal cortex. In detail, all patients shared hypometabolism in the orbitofrontal cortex; inferior, superior and middle frontal gyri; and insula and more variably in the angular gyrus, bilaterally (Fig. 2a). The severity of hypometabolism in the fronto-insular-parietal cortex decreased across phases (from the acute to 7–9-m) (Fig. 1). Specifically, acute, 1-m, 2-m and 5-m patients showed significantly more severe brain hypometabolism than 7–9-m patients ($p_{acute} = 0.000$, $p_{1-m} = 0.001$, $p_{2-m} = 0.001$ and $p_{5-m} = 0.033$). Moreover,
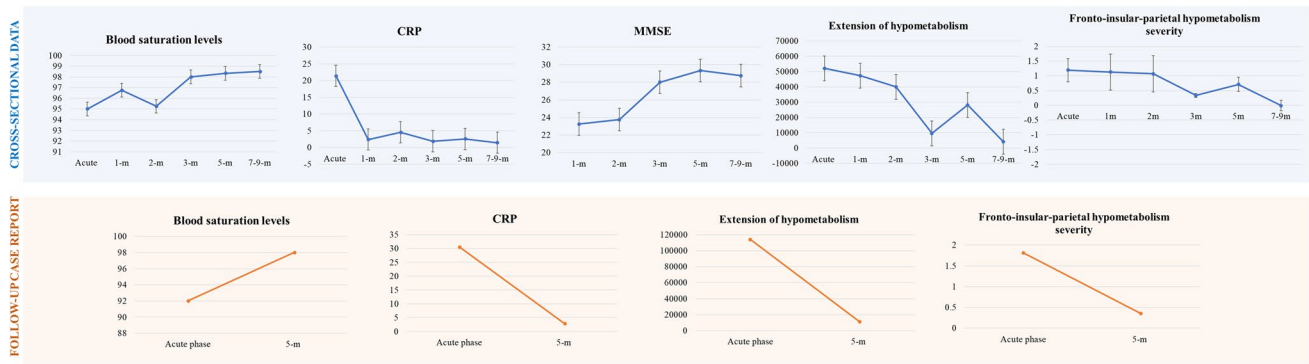
Fig. 1 Clinical values over time: cross-sectional and longitudinal data. The cross-sectional (blue panel) and longitudinal (orange panel) clinical and imaging data show an improvement in the clinical picture of SARS-CoV-2 patients over time

acute, 1-m and 2-m patients featured more severe hypometabolism than 3-m patients ($p_{acute} = 0.003$, $p_{1-m} = 0.013$ and $p_{2-m} = 0.021$) (Table 1).

Hypometabolism SPM maps at the individual level

Patients with acute COVID-19 showed the most severe brain dysfunction, with a widespread and diffuse cortical hypometabolism (Fig. S1). The seven acute patients showed hypometabolism in the frontal cortex, bilaterally (orbitofrontal cortex; inferior, superior and middle frontal gyri; medial pre-frontal cortex) extending to the anterior cingulate cortex, insula, temporal and parietal cortical regions, including precuneus, bilateral angular and supramarginal gyrus. Moreover, a frequent sub-cortical hypometabolism in the thalamus and caudate nuclei was observed. In sub-acute cases (1 month and 2 months), we found similar hypometabolic patterns to the acute phase with widespread involvement of the frontal, temporal and parietal brain regions. Significant recovery was observed in subcortical nuclei. At 3 months, there was a significant reduction of brain hypometabolism with a recovery in the left middle-superior and orbital frontal gyri and parietal regions compared to 2-month patients. See Fig. S2 for sub-acute patients. At 5 months after the infection, we found only a little residual hypometabolic cluster in the right superior and middle frontal cortex and medial frontal cortex. Significant recovery was observed in temporal and anterior cingulate cortices. At 7–9 months, no significant hypometabolic clusters were even present. When we quantified the extension of hypometabolism maps, we found that the hypometabolism decreased during the time (from the acute phase to 7–9 months). See Fig. S3 for sub-acute patients. Acute, 1- and 2-month patients showed significantly more extended brain hypometabolism maps than 7–9-month patients ($p_{acute} = 0.001$, $p_{1-m} = 0.002$ and $p_{2-m} = 0.011$). Moreover, acute and 1-month patients featured

more widespread hypometabolism than 3-month patients ($p_{acute} = 0.009$ and $p_{1-m} = 0.014$) (Fig. 2a, Table 1, Table 3).

Hypermetabolism hallmarks at group level

The commonality analysis showed a massive involvement of brainstem, cerebellum and limbic structures (i.e. amygdala and hippocampus bilaterally) as the hypermetabolic hallmarks, along with more limited involvement of the occipital cortex (Fig. 2b). The severity of hypermetabolism in these regions showed no significant difference across stages (from acute to 7–9-m) (Table 1).

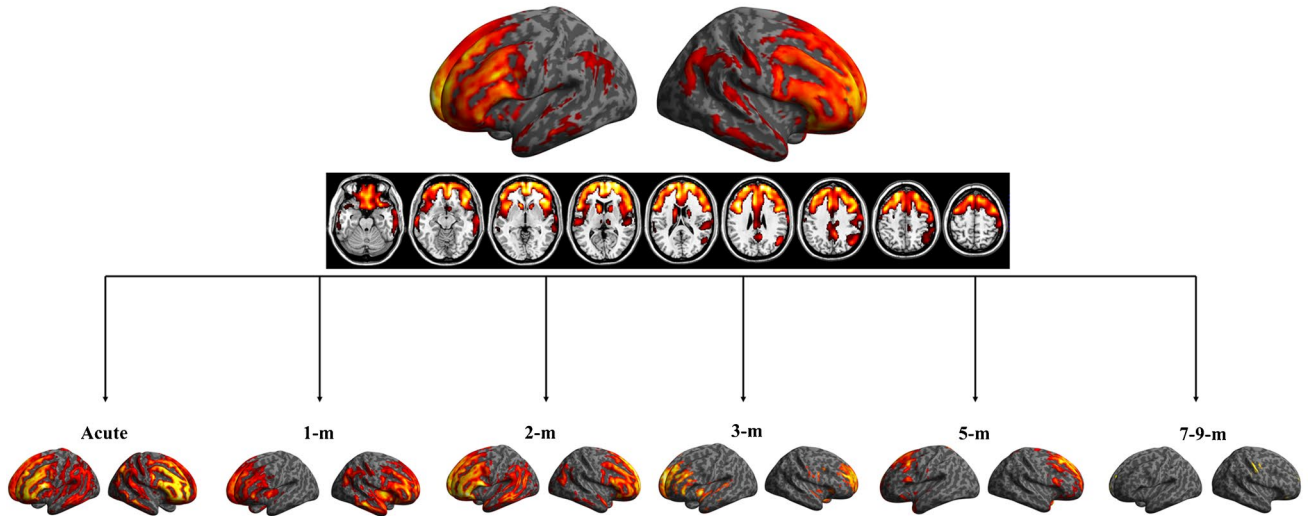### Hypermetabolism SPM maps at the individual level

Concerning the pattern of brain hypermetabolism at single-subject level, all the patients showed a consistent involvement of the brainstem, cerebellum, amygdala, hippocampus and parahippocampus with more variable involvement of occipital regions and sensorimotor cortex (Fig. S1, S2 and S3). The extension of hypermetabolism patterns showed no significant difference over time (Table 1). Of note, an absence of hypo- and hypermetabolism topographical overlap emerged amongst acute, sub-acute and post-COVID-19 groups (S4, Table S4 and Fig. S4).

Longitudinal case study

In the longitudinal case report, the patient with [18F]FDG-PET scans at two-time points (acute and 5-m) showed a pattern of brain functional improvement, similar to those described in the cross-sectional data. In the acute phase, the patient showed a widespread and severe brain hypometabolism affecting all cortical regions and some subcortical structures (bilateral caudate and left thalamus). At 5 months, the same patient showed a nearly complete recovery of brain functionality with residual limited hypometabolic clusters
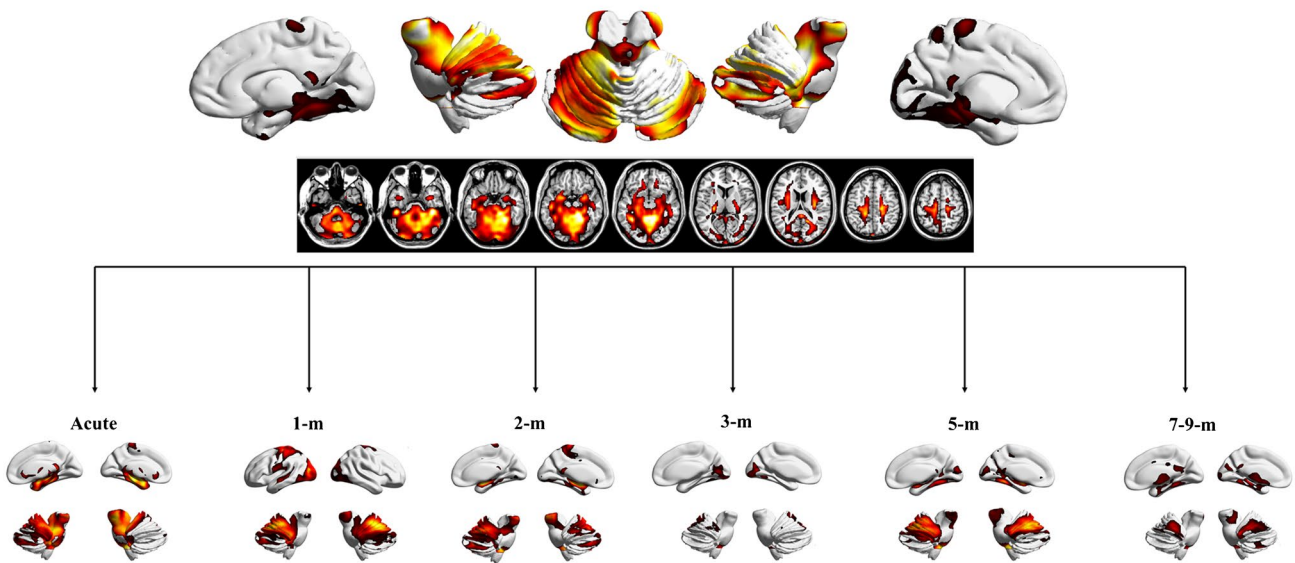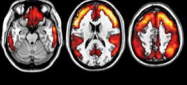
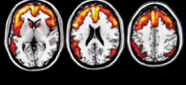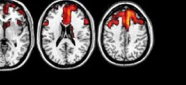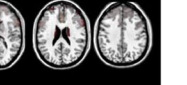**Fig. 2** [^{18}F]FDG-PET brain hypometabolism and hypermetabolism patterns. **a** Commonality pattern of hypometabolism in the whole SARS-CoV-2 group ($p < 0.05$ uncorrected, FWE corrected at the cluster level, k > 100, T-threshold: 1.66) and group-level hypometabolism divided according to the disease phase ($p < 0.05$ uncorrected, FWE corrected at the cluster level, k > 100, T-threshold: 1.66). **b** Commonality pattern of hypermetabolism in the whole SARS-CoV-2 group ($p < 0.05$ uncorrected, FWE corrected at the cluster level, k > 100, T-threshold: 1.66) and group-level hypometabolism divided according to the disease phase ($p < 0.05$ uncorrected, FWE corrected at the cluster level, k > 100, T-threshold: 1.66). Abbreviations: m: months

only in superior and middle frontal cortices, superior medial frontal cortices and caudate nucleus. Both hypometabolism extension and severity of the fronto-insular-parietal cortex decreased from the acute phase to the 5-m follow-up (Fig. 1, Fig. 3a). Concerning the pattern of brain hypermetabolism, in the acute phase, the patient showed severe brain hypermetabolism affecting the brainstem, cerebellum, parahippocampus, hippocampus and amygdala bilaterally. At 5 months, hypermetabolism affecting the cerebellum, occipital and sensorimotor cortex was still present (Fig. 3b). We found no overlap between hypo- and hypermetabolism maps at baseline at two-time points (S4, Table S4 and Fig. S4).

Table 3 Localisation of significant clusters of hypometabolism in each group of patients (SPM analysis—group comparisons)

Acute phase	1-month	2-months	3-months	5-months	7-9-months
Cluster 1 [91137 voxel]	Cluster 1 [69298 voxel]	Cluster 1 [60341 voxel]	Cluster 1 [14821 voxel]	Cluster 1 [35306 voxel]	No significant clusters
T > 1.66	T > 1.66	T > 1.66	T > 1.66	T > 1.66	
B MOF	B MOF	B MOF	B MFG	B MFG	
B SOF	B SOF	B SOF	B SFG	B SFG	
B IFG	B IFG	B IFG	B Insula	B Insula	
B MFG	B MFG	B MFG	ACC	ACC	
B SFG	B SFG	B SFG	L Caudate nucleus	B Caudate nucleus	
ACC	ACC	ACC			
B ITG	R ITG	B ITG			
B MTG	R MTG	B MTG			
B ITG	R ITG	B ITG			
B RO	B Insula	B Insula			
B Insula	R AG	B AG			
B AG	R SUPG				
B Precuneus	R IPG				
B SUPG	B Caudate nucleus				
B IPG	L Thalamus				
	R Putamen				

B bilateral; *L*: left; *R*: right; *MOF*: middle orbitofrontal cortex; *SOF*: superior orbitofrontal cortex; *IFG*: inferior frontal gyrus; *MFG*: middle frontal gyrus; *SFG*: superior frontal gyrus; *ACC*: anterior cingulate cortex; *ITG*: inferior temporal gyrus; *MTG*: middle temporal gyrus; *STG*: superior temporal gyrus; *RO*: rolandic operculum; *SUPG*: supramarginal gyrus; *IPG*: inferior parietal gyrus. This table reports only the significant clusters above the T-threshold of 1.66 ($p < 0.05$ uncorrected at voxel level with K > 100, FWE-corrected at the cluster level)

Correlations between brain hypometabolism and clinical variables

Both hypometabolism map extent and hypometabolism severity in the fronto-insular-parietal cortex significantly correlated with blood saturation levels, CRP, MMSE corrected scores and BMI. Patients with more widespread hypometabolism and severe hypometabolism in the fronto-insular cortex had more severe oxygen desaturation, inflammatory status, global cognitive alteration and higher BMI (Fig. 4). The hypometabolism map extent and hypometabolism severity in the hallmark regions showed a significant correlation with neuropsychological tests belonging to executive/attentive cognitive domains. The severity of hypometabolism in hallmark regions correlated with performance in the ROCF immediate recall test ($p_{hypo} = 0.028$; $\rho = -0.656$). The extension of brain hypometabolism showed a significant correlation with digit forward test scores ($p = 0.026$; $\rho = -0.644$), RAVLT ($p = 0.028$; $\rho = -0.656$) and ROCF immediate recall performance (p = 0.040; $\rho = -0.624$). The brain hypermetabolism extension correlated with CRP; the more extended the hypometabolism pattern, the higher the CRP values ($p = 0.026$; $\rho = 0.437$).

As regards the brain hypometabolism extent, a significant regression model was found ($F (5.13) = 5.009$, $p < 0.009$), with an R^2 of 0.658. We also found a significant inverse association between brain hypometabolism extent and MMSE corrected scores ($\beta = -0.702$; $p = 0.011$) and a significant positive association with CRP ($\beta = 0.563$; $p = 0.028$). Thus, severe cognitive impairment and inflammation status were significantly associated with widespread extension and severity of brain hypometabolic patterns in SARS-CoV-2 patients. Regarding the severity of hypometabolism in the fronto-insular-parietal cortex, a significant regression model was found ($F (5.13) = 10.26$, $p < 0.000$), with an R^2 of 0.798. We found a significant inverse association between hypometabolism and MMSE corrected scores ($\beta = -0.863$; $p = 0.000$) and a significant positive association between hypometabolism and saturation ($\beta = 0.870$; $p = 0.002$) and CRP ($\beta = 0.567$; $p = 0.006$) as well as BMI ($\beta = 0.334$; $p = 0.049$). This means that severe cognitive deterioration, inflammation status, oxygen desaturation and high BMI significantly explained the degree of hypometabolism affecting the fronto-insular-parietal cortex in SARS-CoV-2 patients. As for the brain hypermetabolism in the brainstem, cerebellum and limbic structures, a regression was found ($F (5.13) = 2.966$ $p < 0.056$), with an R^2 of 0.533, where CRP levels significantly predicted the severity of hypermetabolism ($\beta = 0.578$; $p = 0.049$).

Fig. 3 Longitudinal [18F] FDG-PET case report. **a** [18F] FDG-PET single subject hypometabolism and **b** hypermetabolism SPM t-maps in a SARS-CoV-2 patient acquired during the acute phase (left) and after 5 months of follow-up (right)
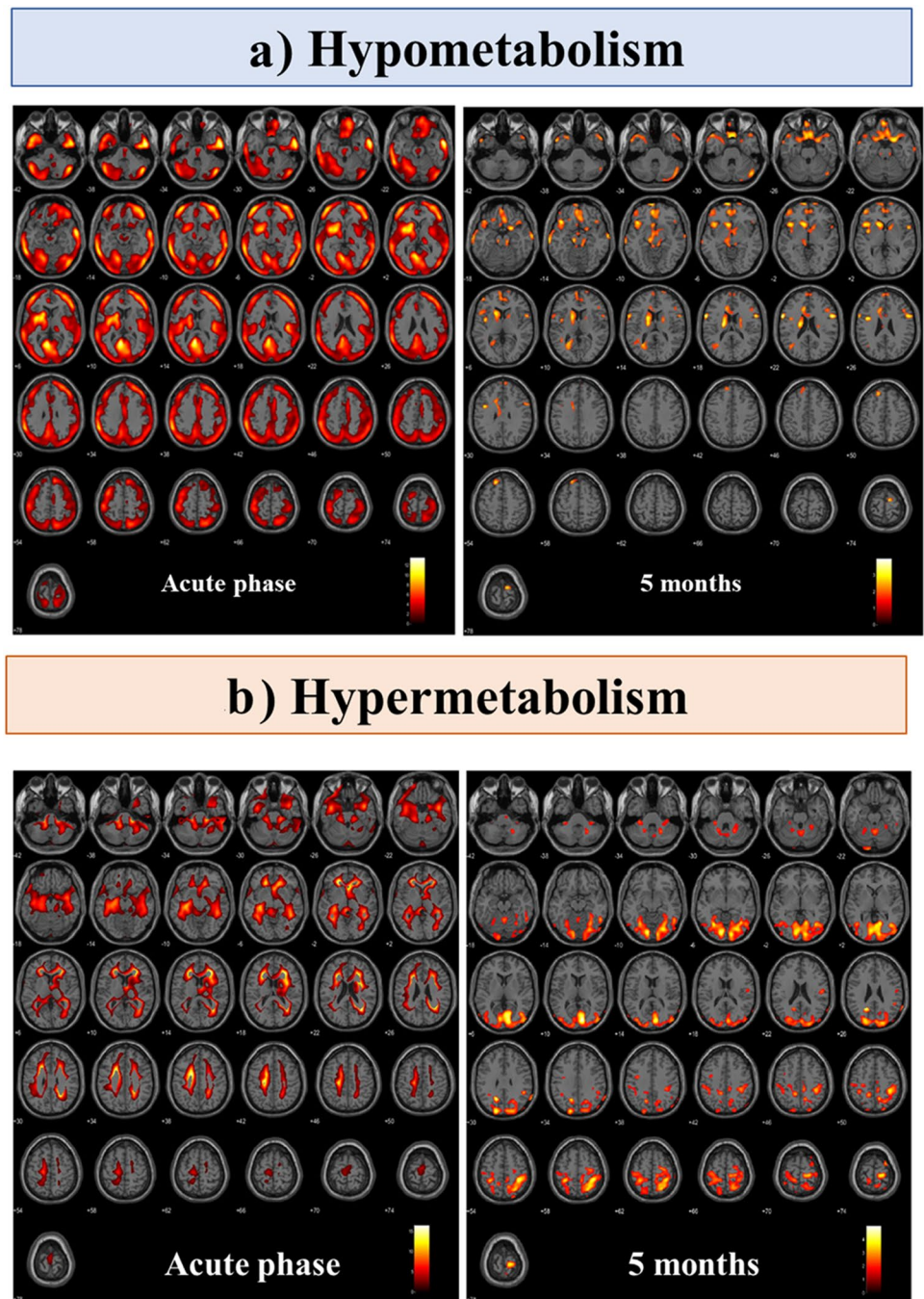

Discussion

The present study investigated the temporal progression of functional brain alterations and their association with clinical/biological parameters in the full-time spectrum of COVID-19-related neurological symptoms by combining cross-sectional and longitudinal approaches. We evaluated the disease's brain metabolic changes in acute and subacute (1-m , 2-m and 3-m) phases and the neuro-post-COVID-19 syndrome (5-m and 7–9-m). We found a consistent fronto-insular hypometabolism in neuro-COVID-19 patients, suggesting its possible vulnerability to the SARS-CoV-2 infection. Cross-sectional and longitudinal cases showed that extension and severity of brain cortical hypometabolism decreased over time (from acute to 7–9-m phases) along with improved blood saturation, systemic inflammation and global cognitive performance. Neuro-COVID-19 patients, after 7–9 months from the infection, presented no longer brain hypometabolism and the saturation levels, CRP and global cognitive performance were within the normal ranges. Brain hypermetabolism mainly
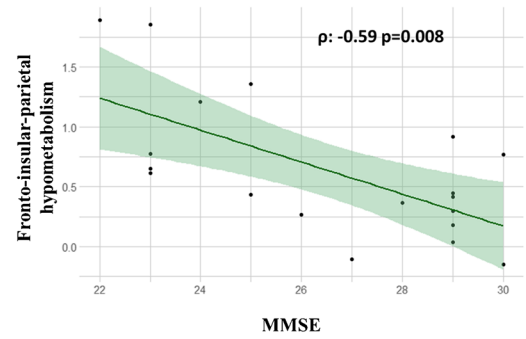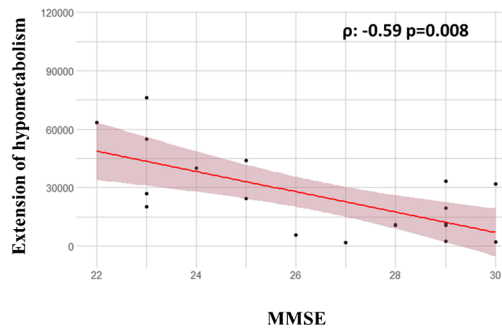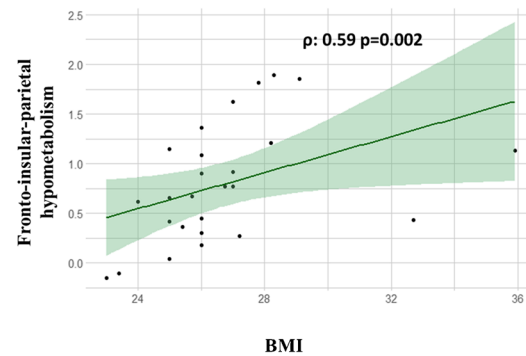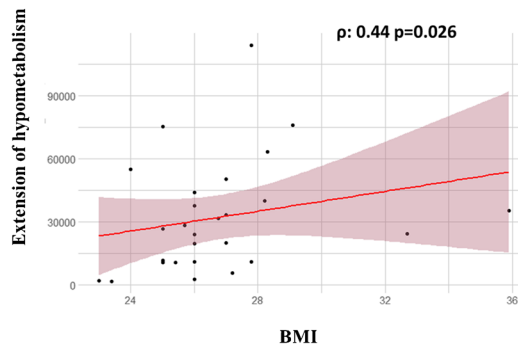
Blood saturation level
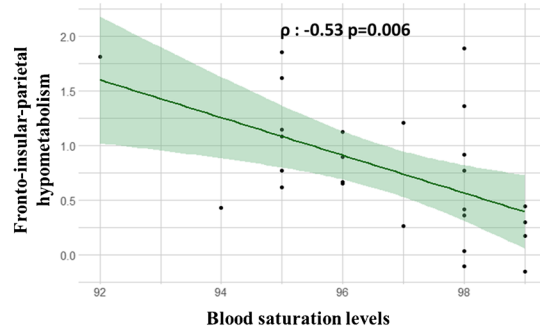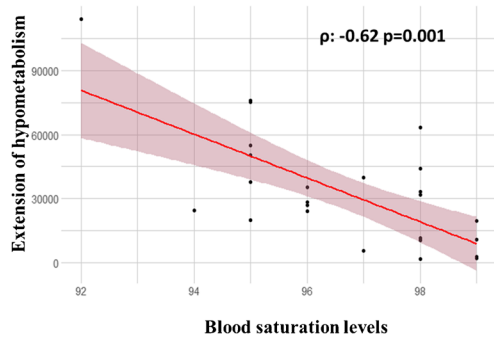
CRP
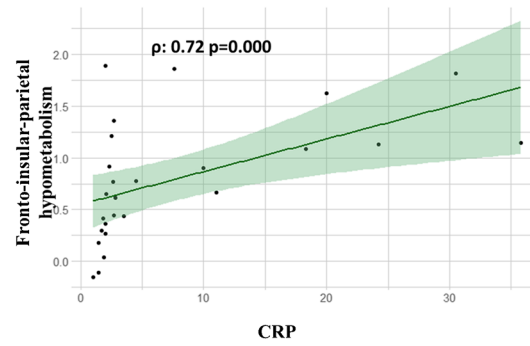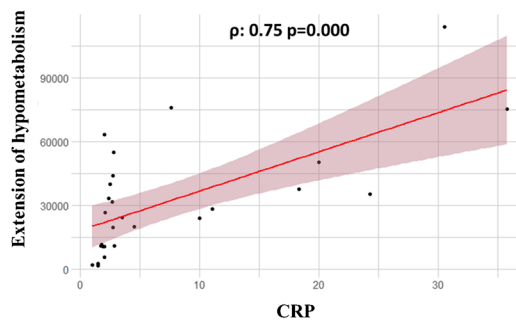
MMSE

BMI

involved the brainstem, cerebellum and limbic structures (amygdala and hippocampus), plus occipital and sensorimotor cortices to a variable extent. Contrary to hypometabolism, brain hypermetabolism persisted over time, up to 7–9 months from the infection. The extent and severity of hypermetabolism were associated with the inflammatory status. These findings suggest that the cortical functional impairment observed in patients with neuro-COVID-19 is likely to be transient and almost reversible. The association with the severity of saturation level and inflammatory body status suggest synergistic effects of systemic virus-mediated inflammation (probably sustained by systemic cytokine release) and transient hypoxia, which could induce dysfunction of neural synaptic activity, which is, however, reversible. On the other hand, the long-lasting brain hypermetabolism in subcortical and limbic structures seems to be an immediate consequence of virus-induced inflammation processes and might represent a neural substrate of the neurological sequelae in post-COVID-19 syndrome.

The brain hypometabolism analyses revealed that the fronto-insular cortex was the most consistently affected region. Thus, it might represent the dysfunctional brain hallmark of CNS involvement in COVID-19 (the so-called neuro-metabolic signature). Previous [^{18}F]FDG-PET findings show that COVID-19 patients with persistent hyposmia isolated or associated with cognitive dysfunction present metabolic abnormalities in core olfactory cortical areas (orbitofrontal cortex) [17, 18, 28–30], frontal cortical areas (superior, middle, inferior frontal cortex) [31] and the insula [16]. Indeed, 96% of our patients reported hyposmia during the acute phase of the disease. According to a heavily debated hypothesis, SARS-CoV-2 neural access could involve the transport of the virus through the nasal cavity and olfactory bulb [32, 33]. This hypothesis is supported by some histopathological findings showing that viral particles are present in neural cell bodies and endothelial cells in the olfactory bulb and frontal cortex (including the orbito-frontal gyri) in COVID-19 patients [34]. However, the predominance of hyposmic and anosmic symptoms observed in our and other studies could also lead to loss of neuron functionality in these olfactory-related brain regions through repeated sensory deprivation, without implying a neuroinvasion mechanism. According to a recent longitudinal study in a large cohort of COVID-19 patients ($N = 401$), the virus would not necessarily need to enter the CNS; anterograde degeneration from olfactory neurons might be sufficient to generate the pattern of abnormalities revealed in imaging findings [35]. The regression over time of functional brain impairments

here further reinforces this hypothesis. The neocortical brain alteration might be a temporary consequence of several factors, including prolonged olfactory impairments that can be reversible. This interpretation is in line with neuropathological findings showing that detectable virus in COVID-19 brains is very low and does not correlate with the histopathological alterations [36].

The brain hypermetabolism evaluation revealed in most patients the involvement of the midbrain, cerebellum, amygdala and hippocampus, variably associated with occipital and sensorimotor cortex. Our results agree with previous findings showing mild hypermetabolism in the vermis, dentate nucleus, pons and the visual cortex in the acute phase of COVID-19 subjects [15]. Whether the hypermetabolism in COVID-19 patients has an artefactual origin or may directly reflect inflammation/infection is still debated [3]. The persistent hypermetabolism in our cohorts, along with the improvement of brain hypometabolism, is in itself a clue against the artefactual origin of the former. In addition, we controlled for the risk of hypermetabolism artefact due to the proportional scaling procedure for intensity normalisation [25, 26]. No differences between patients and HC emerged, excluding the overestimation of hypermetabolism (Table S2) and suggesting a biological meaning for hypermetabolism in the patients. In addition, we found a significant association between hypermetabolism extent/severity and the inflammatory status, suggesting that hypermetabolism can be part of the inflammatory response to SARS-CoV-2 infection more than a mere artefact. Indeed, the pathophysiology of hypermetabolism has been previously found and discussed in diseases where brain inflammation is expected (e.g. autoimmune encephalitis) [7].

Our cross-sectional and longitudinal brain imaging data showed that brain dysfunctions are more severe and extended during the acute phase, decreasing progressively. Specifically, we found the first significant improvement of brain functionality after 3 months from the SARS-CoV-2 infection and further on at 5 months. The hypometabolism disappeared at 7–9 months. The case–control patient followed longitudinally in the acute phase, and at 5 months, follow-up showed the same pattern of brain functional improvement. These data are congruent with the neuropsychological profiles of patients; indeed, only sub-acute patients at 1 and 2 months after infection presented pathological scores in executive tests (Table 2). Our findings are consistent with the previous longitudinal [^{18}F]FDG-PET study on COVID-19-related encephalopathy, where the widespread brain hypometabolism in the acute phases—including the fronto-insular cortex—improved at 6 months of follow-up [11]. Similarly, Blazhenets et al. demonstrated a slow recovery of neocortical dysfunction and cognitive dysfunctions (6 months after a SARS-CoV-2 infection) [12]. Of note, we provide for the first time a picture of brain functioning 9 months after the infection, demonstrating a complete brain functional recovery.

Along with brain metabolism, global cognitive functioning, blood saturation and inflammatory status gradually improved over time. Of note, widespread and severe hypometabolism was associated with severe SatO2, CRP, global cognitive deterioration and higher BMI. This result suggests that inflammation status, oxygen desaturation and BMI may significantly influence the degree of brain hypometabolism and related cognitive deterioration. On the contrary, brain hypermetabolism did not change significantly from the acute phase to post-COVID-19 syndrome. This long-lasting brain hypermetabolism can be caused by the well-documented sustained immune response to the virus, and it might represent a neural substrate of neurological sequelae in post-COVID-19 syndrome [37]. Long-lasting hypermetabolism might result from a complex interplay between brain hypometabolism and hypermetabolism. However, in our cohort, the overlap between hypo- and hypermetabolism maps in both cross-sectional and longitudinal data was absent, thus, not supporting a hypometabolism/hypermetabolism transition (Tables S3-S4). Future studies with more longitudinal data are needed to test this hypothesis properly. Our results support the hypothesis that several indirect pathogenetic mechanisms—e.g. virus-mediated inflammation sustained by systemic cytokine release and transient hypoxia—may sustain the observed widespread synaptic dysfunction [34, 37]. In this context, we also found that high BMI could also represent a negative prognostic factor for neurological impairment. Patients with obesity are more prone to developing altered respiratory states, diabetes, hypertension, cardiovascular diseases and low-grade chronic inflammation, making them susceptible to poorer outcomes [38].

Some of the limitations of this study include the small sample size and lack of longitudinal measures. We used a cross-sectional approach to describe possible time-dependent changes in brain metabolism, and even though the longitudinal case study confirmed the cross-sectional results, future longitudinal evaluations in large cohorts are necessary. In addition, we could perform a standardised neuropsychological battery only on a sub-group of patients. Thus, caution is required in the interpretation of the present results, especially in terms of generalizability. In order to provide generalisable findings about the CNS involvement in COVID-19, brain metabolic changes should be evaluated in a longitudinal setting with large cohorts of patients clinically and neuropsychologically well evaluated over a long time, and with the inclusion of asymptomatic, mild-moderate and severe manifestations of COVID-19, in a comprehensive age range. A big data approach is essential to estimate the prevalence of neurological manifestation and functional brain alteration in COVID-19.

In conclusion, the present functional neuro-imaging PET study suggests that the fronto-insular cortex can be considered a neuro-metabolic signature of CNS involvement by COVID-19. Cross-sectional and longitudinal data demonstrated that cortical functional impairment observed in patients with neuro-COVID-19 infection is likely to be transient and almost reversible. Systemic virus-mediated inflammation and transient hypoxia may induce reversible neural dysfunctions, whereas brain hypermetabolism seems to be long-lasting and related to the persistent inflammation processes.

Declarations

References

1. Vakili K, Fathi M, Hajiesmaeili M, Salari M, Saluja D, Tafakhori A, et al. Neurological symptoms, comorbidities, and complications of COVID-19: a literature review and meta-analysis of observational studies. Eur Neurol Karger Publishers. 2021;84:307–24.

2. Schweitzer F, Kleineberg NN, Göreci Y, Onur OA, Franke C, Warnke C. Neuro-COVID-19 is more than anosmia: clinical presentation, neurodiagnostics, therapies, and prognosis. Curr Opin Neurol LWW. 2021;34:423–31.

3. Meyer PT, Hellwig S, Blazhenets G, Hosp JA. Molecular imaging findings on acute and long-term effects of COVID-19 on the brain: a systematic review. J Nucl Med Soc Nuclear Med. 2022;63:971–80.

4. Soriano JB, Murthy S, Marshall JC, Relan P, Diaz J V, Group WHOCCDW. A clinical case definition of post-COVID-19 condition by a Delphi consensus. Lancet Infect Dis. Elsevier. 2021;22:e102–7.

5. Moghimi N, Di Napoli M, Biller J, Siegler JE, Shekhar R, McCullough LD, et al. The neurological manifestations of post-acute sequelae of SARS-CoV-2 infection. Curr Neurol Neurosci Rep Springer. 2021;21:1–17.

6. Aghagoli G, Gallo Marin B, Katchur NJ, Chaves-Sell F, Asaad WF, Murphy SA. Neurological involvement in COVID-19 and potential mechanisms: a review. Neurocrit Care Springer. 2021;34:1062–71.

7. Yachou Y, El Idrissi A, Belapasov V, Ait BS. Neuroinvasion, neurotropic, and neuroinflammatory events of SARS-CoV-2:

understanding the neurological manifestations in COVID-19 patients. Neurol Sci Springer. 2020;41:2657–69.

8. DosSantos MF, Devalle S, Aran V, Capra D, Roque NR, Coelho-Aguiar J de M, et al. Neuromechanisms of SARS-CoV-2: a review. Front Neuroanat Front. 2020;37.

9. Gasmi A, Tippairote T, Mujawdiya PK, Gasmi Benahmed A, Menzel A, Dadar M, et al. Neurological involvements of SARS-CoV2 infection. Mol Neurobiol Springer. 2021;58:944–9.

10. Rudroff T, Workman CD, Ponto LLB. 18F-FDG-PET imaging for post-COVID-19 brain and skeletal muscle alterations. Viruses. Multidisciplinary Digital Publishing Institute. 2021;13:2283.

11. Kas A, Soret M, Pyatigoskaya N, Habert M-O, Hesters A, Le Guennec L, et al. The cerebral network of COVID-19-related encephalopathy: a longitudinal voxel-based 18F-FDG-PET study. Eur J Nucl Med Mol Imaging. Springer. 2021;48:2543–57.

12. Blazhenets G, Schroeter N, Bormann T, Thurow J, Wagner D, Frings L, et al. Slow but evident recovery from neocortical dysfunction and cognitive impairment in a series of chronic COVID-19 patients. J Nucl Med Soc Nuclear Med. 2021;62:910–5.

13. Hosp JA, Dressing A, Blazhenets G, Bormann T, Rau A, Schwabenland M, et al. Cognitive impairment and altered cerebral glucose metabolism in the subacute stage of COVID-19. Brain Oxford University Press. 2021;144:1263–76.

14. Dressing A, Bormann T, Blazhenets G, Schroeter N, Walter LI, Thurow J, et al. Neuropsychological profiles and cerebral glucose metabolism in neurocognitive long COVID-syndrome. J Nucl Med: Society of Nuclear Medicine. 2021;63:1058–63.

15. Sollini M, Morbelli S, Ciccarelli M, Cecconi M, Aghemo A, Morelli P, et al. Long COVID hallmarks on [18F] FDG-PET/CT: a case-control study. Eur J Nucl Med Mol Imaging. Springer. 2021;48:3187–97.

16. Donegani MI, Miceli A, Pardini M, Bauckneht M, Chiola S, Pennone M, et al. Brain metabolic correlates of persistent olfactory dysfunction after SARS-Cov2 infection. Biomedicines. Multidisciplinary Digital Publishing Institute. 2021;9:287.

17. Delorme C, Paccoud O, Kas A, Hesters A, Bombois S, Shambrook P, et al. COVID-19-related encephalopathy: a case series with brain FDG-positron-emission tomography/computed tomography findings. Eur J Neurol Wiley Online Library. 2020;27:2651–7.

18. Niesen M, Trotta N, Noel A, Coolen T, Fayad G, Leurkin-Sterk G, et al. Structural and metabolic brain abnormalities in COVID-19 patients with sudden loss of smell. Eur J Nucl Med Mol Imaging. Springer. 2021;48:1890–901.

19. Caminiti SP, Sala A, Presotto L, Chincarini A, Sestini S, Perani D, et al. Validation of FDG-PET datasets of normal controls for the extraction of SPM-based brain metabolism maps. Eur J Nucl Med Mol Imaging. Springer. 2021;1–14.

20. Paez D, Gnanasegaran G, Fanti S, Bomanji J, Hacker M, Sathekge M, et al. COVID-19 pandemic: guidance for nuclear medicine departments. Eur J Nucl Med Mol Imaging. 2020;47:1615–1619.

21. Varrone A, Asenbaum S, Vander Borght T, Booij J, Nobili F, Någren K, et al. EANM procedure guidelines for PET brain imaging using [18F]FDG, version 2. Eur J Nucl Med Mol Imaging. 2009;36:2103–10.

22. Della Rosa PA, Cerami C, Gallivanone F, Prestia A, Caroli A, Castiglioni I, et al. A standardized [18F]-FDG-PET template for spatial normalization in statistical parametric mapping of dementia. Neuroinformatics Springer. 2014;12:575–93.

23. Kogan R V, de Jong BA, Renken RJ, Meles SK, van Snick PJH, Golla S, et al. Factors affecting the harmonization of disease-related metabolic brain pattern expression quantification in [18F] FDG-PET (PETMETPAT). Alzheimer's Dement Diagnosis, Assess Dis Monit. Elsevier. 2019;11:472–82.

24. Perani D, Della Rosa PA, Cerami C, Gallivanone F, Fallanca F, Vanoli GE, et al. Validation of an optimized SPM procedure for FDG-PET in dementia diagnosis in a clinical setting. NeuroImage Clin. Elsevier B.V. 2014;6:445–54.

25. Friston KJ. Statistical parametric mapping. Neurosci Databases. Springer. 2003. p. 237–50.

26. Buchert R, Wilke F, Chakrabarti B, Martin B, Brenner W, Mester J, et al. Adjusted scaling of FDG positron emission tomography images for statistical evaluation in patients with suspected Alzheimer's disease. J Neuroimaging Wiley Online Library. 2005;15:348–55.

27. Presotto L, Ballarini T, Caminiti SP, Bettinardi V, Gianolli L, Perani D. Validation of 18 F-FDG-PET single-subject optimized SPM procedure with different PET scanners. Neuroinformatics Springer. 2017;15:151–63.

28. Morand A, Campion J-Y, Lepine A, Bosdure E, Luciani L, Cammilleri S, et al. Similar patterns of [18F]-FDG brain PET hypometabolism in paediatric and adult patients with long COVID: a paediatric case series. Eur J Nucl Med Mol Imaging. Springer. 2022;49:913–20.

29. Guedj E, Million M, Dudouet P, Tissot-Dupont H, Bregeon F, Cammilleri S, et al. 18F-FDG brain PET hypometabolism in post-SARS-CoV-2 infection: substrate for persistent/delayed disorders. Eur J Nucl Med Mol Imaging Springer. 2021;48:592–5.

30. Guedj E, Campion JY, Dudouet P, Kaphan E, Bregeon F, Tissot-Dupont H, et al. 18F-FDG brain PET hypometabolism in patients with long COVID. Eur J Nucl Med Mol Imaging. Springer. 2021;48:2823–33.

31. Karimi-Galougahi M, Yousefi-Koma A, Bakhshayeshkaram M, Raad N, Haseli S. 18FDG PET/CT scan reveals hypoactive orbitofrontal cortex in anosmia of COVID-19. Acad Radiol. Elsevier. 2020;27:1042.

32. Seshadri S, De Erausquin GA, Snyder H, Hosseini AA, Brugha TS, Carrillo M, et al. The chronic neuropsychiatric sequelae of COVID-19: the need for a prospective study of viral impact on brain functioning. Wiley. 2020.

33. Meinhardt J, Radke J, Dittmayer C, Franz J, Thomas C, Mothes R, et al. Olfactory transmucosal SARS-CoV-2 invasion as a port of central nervous system entry in individuals with COVID-19. Nat Neurosci Nature Publishing Group. 2021;24:168–75.

34. Paniz-Mondolfi A, Bryce C, Grimes Z, Gordon RE, Reidy J, Lednicky J, et al. Central nervous system involvement by severe acute respiratory syndrome coronavirus-2 (SARS-CoV-2). J Med Virol Wiley Online Library. 2020;92:699–702.

35. Douaud G, Lee S, Alfaro-Almagro F, Arthofer C, Wang C, McCarthy P, et al. SARS-CoV-2 is associated with changes in brain structure in UK Biobank. Nature. Nature Publishing Group. 2022;1–17.

36. Thakur KT, Miller EH, Glendinning MD, Al-Dalahmah O, Banu MA, Boehme AK, et al. COVID-19 neuropathology at Columbia University Irving Medical Center/New York Presbyterian Hospital. Brain [Internet]. 2021;144:2696–708. Available from: https://doi.org/10.1093/brain/awab148

37. Files JK, Sarkar S, Fram TR, Boppana S, Sterrett S, Qin K, et al. Duration of post–COVID-19 symptoms is associated with sustained SARS-CoV-2–specific immune responses. JCI insight. Am Soc Clin Investig. 2021;6.

38. Hendren NS, de Lemos JA, Ayers C, Das SR, Rao A, Carter S, et al. Association of body mass index and age with morbidity and mortality in patients hospitalized with COVID-19: results from the American Heart Association COVID-19 Cardiovascular Disease Registry. Circ Am Heart Assoc. 2021;143:135–44.